

Measuring dispersion of biphotons

Assaf Barak and Mordechai Segev

Physics Department, Technion–Israel Institute of Technology, Haifa 32000, Israel

(Received 19 February 2012; published 26 October 2012)

We study the interference pattern of biphotons passing through a dispersive medium, and devise a method for measuring dispersion in coincidence counting of entangled photons. By measuring the Gouy phase shift accompanying dispersion, we show that it fundamentally differs from the Gouy phase expected from classical models. Finally, we show that the second-order correlation function of the dispersed biphoton can be much wider than the pattern predicted from classical analog.

DOI: [10.1103/PhysRevA.86.043838](https://doi.org/10.1103/PhysRevA.86.043838)

PACS number(s): 42.50.Nn, 42.50.Dv, 42.50.St

It is well known that when path-entangled photons pass through a dispersive medium the temporal width of their wave packet gets broader due to dispersion. However, this broadening, which is usually dominated by group velocity dispersion (GVD) does not reveal itself in coincidence counts experiments, due to dispersion cancellation [1,2]. In practice, in two-photon interference experiments [2], measurements are made with detectors with response time much longer than the temporal width of the biphoton wave packet. In this setting, one measures the coincidence counting rate by integrating over the second-order correlation function. The temporal integration cancels out the GVD information, and the interference pattern appears as if the photons did not pass through a dispersive medium whatsoever. To overcome this difficulty, it was suggested to measure the correlation function without the temporal integration, which means that the temporal width of the biphoton must be much wider than the response time of the detection system. This idea was indeed implemented by making use of the “start-stop” method, to demonstrate the broadening of the correlation function of entangled photons propagating in fibers [3], the two-photon interference of dispersed biphotons [4], and nonlocal dispersion cancellation [5]. However, in all these experiments the resolution time of the detection system was of the order of hundreds of picoseconds. Thus, the biphoton wave packet had to broaden to nanoseconds. A different approach recently used frequency up-conversion to detect dispersion effects on the conversion efficiency [6]. However, while such approach indeed yields a better time resolution (femtosecond scale resolution), it requires a high flux of photon pairs to get reasonable conversion efficiency. Finally, a recent proposition suggested a novel interferometer enabling dispersion cancellation of even and odd orders without being restricted by electronic resolutions, or by the efficiency of nonlinear processes (which is inevitably small at a small flux of photons) [7]. That proposed interferometer combines Hong-Ou-Mandel (HOM) with Mach-Zehnder (MZ) interferometers. In such an interferometer, one can observe, in different regimes, odd and even dispersion effects in the coincidence count rate. While observing odd dispersion effects is well understood and was observed experimentally [8], the observation of even-order dispersion effects is novel, and it originates from interference between two quantum amplitudes inside the MZ interferometer. Basically, there are two indistinguishable amplitudes that interfere; one describing

two photons evolving inside a dispersive medium (one arm of the interferometer), the other describing two photons evolving in free space (second arm of the interferometer). This is in contrast to the HOM interferometer where the two interfering amplitudes accumulate the same phase, and thus dispersion is not manifested in the interference pattern. This type of proposed interferometer raises new questions about the dispersive nature of biphotons. For example, will the measurement of biphoton dispersion yield the same results as their classical analogs, or will they differ?

Here, we discuss a different type of interferometer, designed to measure biphoton dispersion by interfering different quantum amplitudes. We find fundamental deviations from classical optics. First, we find that an additional phase that always accompanies the optical wave packet manifests itself differently for a classical and a biphoton wave packet. This phase appears for Gaussian pulses at their first stages of evolution [9], and it is completely analogous to the Gouy phase appearing for a spatial Gaussian beam as it passes through its waist (due to the uncertainty principle between momentum and space [10]). As such, we will refer to it as the Gouy phase. However, we emphasize that this phase is not an outcome of spatial propagation through the waist of a spatial Gaussian beam; rather, this phase accompanying the biphoton wave packet arises solely from the chromatic dispersion. This equivalence between this biphoton Gouy phase and the spatial Gouy phase of Gaussian beams results from the analogy between the paraxial equation describing beam diffraction in space and the equation describing the evolution of the slowly-varying-amplitude of a temporal pulse in the presence of chromatic dispersion. In addition, we show that the coincidence count measured in this interferometer for the biphoton wave packet can vary dramatically between two extreme cases: (a) dispersion cancellation of the biphoton wave packet while classical pulses exhibit broadening; (b) negligible dispersion of classical pulses while the biphoton exhibits broadening due to dispersion.

Theory. Our interferometer is described in Fig. 1(a). Two entangled photons are generated from a type-I BBO crystal by pumping the crystal with cw light. The crystal is designed to produce two degenerate noncollinear photons. The output polarization is denoted as horizontal (H). Then, one photon is passed through a half wave plate to rotate its polarization to vertical (V), and subsequently it is passed through a controlled delay line with relative delay of τ_0 . The two photons, one in

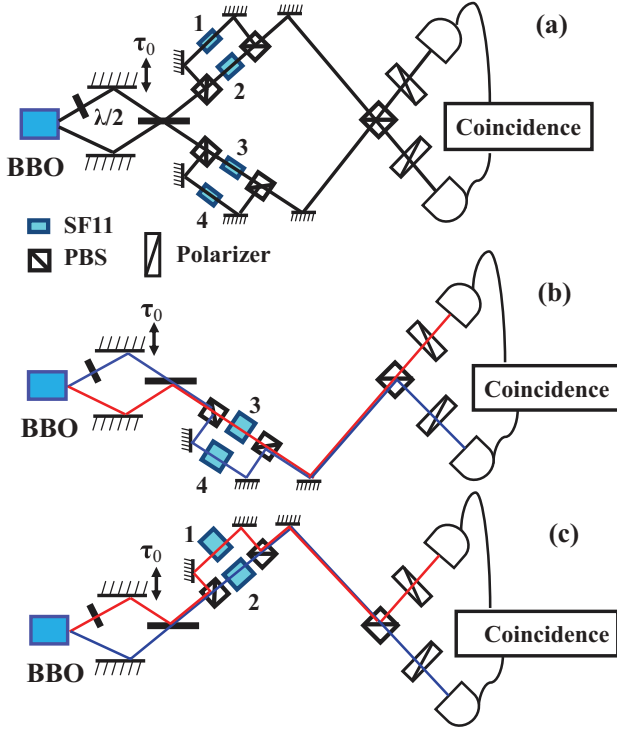


FIG. 1. (Color online) (a) Experimental system. (b), (c) The two interfering quantum paths, presented individually. Red and blue lines mark the paths taken by the two photons.

each arm, then enter a beam splitter (BS), which couples them into a MZ interferometer. In each arm of the interferometer, we split the paths taken by the V and the H photons by means of a polarizing beam splitter (PBS). In each of these paths we may place a sample of SF11 glass of a different thickness, such that GVD will be different in the different paths. The four paths are labeled 1–4. Then, we recombine the paths in each MZ arm

by a PBS. Finally, the fields from the MZ arms are directed to the detectors by a PBS. The purpose of the final PBS placed in front of the detectors, combined with the initial rotation of one of the photons, is to filter out unwanted events. To explain that, notice that inside the MZ interferometer there are four possible quantum amplitudes, two of which describe one photon in one arm while the second photon is in the other arm. These two are unwanted amplitudes, as the GVD phase accumulated by these amplitudes is identical, and thus their interference will not contribute to the GVD measurement. This is exactly the purpose of the last PBS placed in front of the detectors: It filters out the possibility of measuring the interference between amplitudes describing one photon in each arm of the MZ. That is, if the photons go through different arms of the MZ, they enter the same detector and never contribute to the coincidence counts. Thus, this system ensures that we only interfere the two amplitudes where the two photons take the same MZ arm [Figs. 1(b) and 1(c)]. We place polarizers before the two detectors oriented in the direction $H + V$ to fuse the different amplitudes, thereby erasing any “which path” information that results from polarization. The biphoton wave packet just after the photon passed the half wave plate is therefore

$$|\psi\rangle = \int d\Omega \phi(\Omega) a_{\Omega,V}^\dagger a_{-\Omega,H}^\dagger |0\rangle, \quad (1)$$

where $\phi(\Omega)$ is the spectral amplitude, and $a_{\pm\Omega,n}^\dagger$ is the field creation operator in polarization n and frequency $\omega_p/2 \pm \Omega$, and ω_p is the pump frequency. The second-order correlation function is $G^{(2)}(t_1, t_2) = |\langle 0 | \hat{E}_2^{(+)}(t_2) \hat{E}_1^{(+)}(t_1) | \psi \rangle|^2$, where the electric field operator at detector i at time t_i is defined as: $\hat{E}_i^{(+)}(t_i) = \sum_{n=H\pm V} \int d\Omega a_{\Omega,n}^\dagger e^{-i\Omega t_i}$. For a stationary source, the correlation function depends only on $\tau = t_2 - t_1$. To calculate the coincidence count rate, we integrate the second-order correlation function over τ , namely, $R_Q(\tau_0) = \int_{-\infty}^{\infty} G^{(2)}(\tau) d\tau$, to get

$$R_Q(\tau_0) = \frac{1}{8} \left\{ \int d\Omega |\phi(\Omega)|^2 - \text{Re} \left[\int \phi(\Omega) \phi^*(-\Omega) e^{i\frac{\Omega}{c}[L_2-L_1+L_3-L_4]} e^{i\Omega^2[T_1^2+T_2^2-T_3^2-T_4^2]} e^{2i\Omega\tau_0} \right] \right\}. \quad (2)$$

Here, c is the vacuum speed of light, L_i is the optical path for a photon that has passed through path i (experiencing GVD inside the relevant dispersive medium), $T_i = \sqrt{\beta_i^{(2)} z_i}/2$ is the characteristic dispersion time, $\beta_i^{(2)}$ is the second-order dispersion coefficient, and z_i is the length of the dispersive sample in path i . In this paper, we study only positive dispersion ($\beta_i^{(2)} \geq 0$), but this system can be used to study negative dispersion as well. The negative sign before the interference term results from tuning the system to have a π phase difference between the two amplitudes. We assume, for simplicity, that the joint spectral amplitude has a Gaussian shape:

$$\phi(\Omega) = \left(\frac{T^2}{\pi} \right)^{1/4} e^{-\frac{\Omega^2 T^2}{2}}. \quad (3)$$

T is the initial temporal width. We adjust the optical paths to have approximately equal length so $\frac{L_2-L_1+L_3-L_4}{c} \ll T$, and thus the additional phase can be neglected when evaluating the integral in Eq. (2). Substituting Eq. (3) into Eq. (2) one finds

$$R_Q(\tau_0) = \frac{1}{8} \left\{ 1 - \frac{T}{(T^4 + 4T_D^4)^{1/4}} e^{-\frac{\tau_0^2}{T^2 + (2T_D^2/T)^2}} \cos \left[2 \frac{\tau_0^2}{(2T_D)^2 + (T^2/T_D)^2} - \varphi_{G,Q} \right] \right\}, \quad (4)$$

where we defined the dispersion time as $T_D = \sqrt{(T_4^2 + T_3^2 - T_2^2 - T_1^2)}/2$, and the Gouy phase is $\varphi_{G,Q} = \frac{1}{2} \tan^{-1}(2T_D^2/T^2)$.

We now examine two features of the coincidence count rate function: the width, and the equal-path visibility. The width of the Gaussian envelope scales as $\Delta\tau_0 \sim \sqrt{T^2 + (2T_D^2/T)^2}$. The coherent addition of the GVD contributions from all four paths results in an interference pattern of a width that can be varied from T (complete dispersion cancellation) to wider widths, according to the dispersion within each path. The equal-path visibility ($\tau_0 = 0$) decreases when the width of the dip increases. For strong dispersion ($T_D > T$), the Gouy phase saturates as $\varphi_{G,Q} \rightarrow \frac{\pi}{4}$. This gives the visibility

$$\mathcal{V}_Q = \frac{R_Q(\infty) - R_Q(0)}{R_Q(\infty)} = \frac{T}{4T_D}. \quad (5)$$

Notice that the visibility is not zero, the reason being the Gouy phase inside the cosine function in Eq. (4). Since for long propagation distances it takes the value $\pi/4$, the cosine function does not vanish, and a dip is always present. This enables a direct experimental observation of the Gouy phase

$$R_C(\tau_0) = \frac{I^2}{8} \left(2 - \frac{T^2}{(T^4 + 4T_{13}^4)^{1/4} (T^4 + 4T_{24}^4)^{1/4}} e^{-\frac{\tau_0^2}{4} \left[\frac{1}{T^2 + (T_{13}^2/T)^2} + \frac{1}{T^2 + (T_{24}^2/T)^2} \right]} \times \cos \left\{ \frac{\tau_0^2}{4} \left[\frac{1}{T_{13}^2 + (T^2/T_{13})^2} + \frac{1}{T_{24}^2 + (T^2/T_{24})^2} \right] - \varphi_{G,C} \right\} \right). \quad (6)$$

Here we again assumed that the system is tuned to have a π phase difference between the interference terms. Also, the interferometer is adjusted such that the four optical paths are approximately identical in length. Defining the pulse intensity, $I = |E_0|^2$, the dispersion times, $T_{mn} = \sqrt{T_m^2 - T_n^2}$, and the Gouy phase $\varphi_{G,C} = \frac{1}{2} [\tan^{-1}(\frac{T_{13}^2}{T^2}) + \tan^{-1}(\frac{T_{24}^2}{T^2})]$, we again examine the width of the interference term and the equal-path visibility. The width scales as

$$\Delta\tau_0 \sim 2 \sqrt{\frac{[T^2 + (T_{13}^2/T)^2][T^2 + (T_{24}^2/T)^2]}{2T^2 + (T_{13}^2/T)^2 + (T_{24}^2/T)^2}}.$$

Unlike the biphoton case, here there is no coherent addition between the four paths. To get dispersion cancellation, the relative GVD between paths 1 and 3 (and paths 2 and 4) must be equal. Thus, it is possible to design a system where a biphoton will not exhibit dispersion in the coincidence measurement whereas the interference pattern in the coincidence experiment for the corresponding classical pulses will broaden. Interestingly, the opposite scenario is also possible: where the biphotons exhibit dispersion while the measured classical dispersion is approximately zero. To do that, consider a case where $T_{24} \gg T$, while $T_{13} = 0$. Now, for the quantum state the width of the envelope is $\Delta\tau_0 \sim \sqrt{T^2 + (T_{24}^2/T)^2}$, but for the classic pulses we find $\Delta\tau_0 \rightarrow 2T$, that is, the width of the interference term for the classical pulses is narrow as if dispersion is zero, while the wave packet of the biphoton experiences dispersion broadening. In this system,

of biphotons. We emphasize that experimental setups used in previous work [3–6] fundamentally cannot be used for observing the biphoton Gouy phase. This is because in such setups only the modulus of the Glauber function is measured, for which the Gouy phase cancels out. In contradistinction with earlier work, in our setup we interfere the dispersed biphoton from various paths such that the Gouy phase will not disappear when calculating the Glauber function, nor will it cancel out in the coincidence count rate.

For comparison, we calculate the classical analog for this system, where two pulses with randomly fluctuating phases enter the system. We calculate the coincidence count rate of the system as $R_C(\tau_0) = \int_{-\infty}^{\infty} \int_{-\infty}^{\infty} G^{(2)}(t_1, t_2) dt_1 dt_2$. Assuming the initial pulse has Gaussian spectral amplitude, $\phi(\Omega) = E_0(\frac{T}{\pi})^{1/4} e^{-(\Omega^2 T^2)/2}$ (where Ω is the detuning from the central frequency of the pulse, T is the initial temporal width of the pulse and E_0 is the electric field amplitude), gives the following result:

the biphoton wave packet exhibits dispersion broadening while classical pulses display zero dispersion in correlation measurements. The origin for this is the fact that classically the interference dip is restricted by the narrower pulse. If the pulse entering one detector is much narrower than the one entering the second detector (e.g., if it did not pass a dispersive material at all while the other one did), it will dictate the width of the dip. For biphotons, the two-photon wave packet is the entity experiencing dispersion, and thus the dispersion affects both detectors simultaneously. Thus, it is impossible that the field entering one detector will restrict the broadening—as it does with classical pulses.

The equal-path visibility may also exhibit considerable differences between the quantum and classical experiments. For example, consider a case where we place dispersive samples such that $T_{24}, T_{13} \gg T$. Now, the Gouy phase for the classical pulses takes the value $\varphi_{G,C} \rightarrow \frac{\pi}{2}$. The equal-path visibility for this case is

$$\mathcal{V}_C = \frac{R_C(\infty) - R_C(0)}{R_C(\infty)} \rightarrow 0. \quad (7)$$

Thus, whereas for classical pulses the correlations may vanish (Poisson statistics) for $\tau_0 = 0$, for the same setting the biphotons exhibit a dip (bunching). This is again because the biphoton dispersion results from all paths, while for the classical pulses it does not, and thus the additional Gouy phase is different. This setting allows us to observe the Gouy phase of biphotons, and to distinguish it from classic pulses.

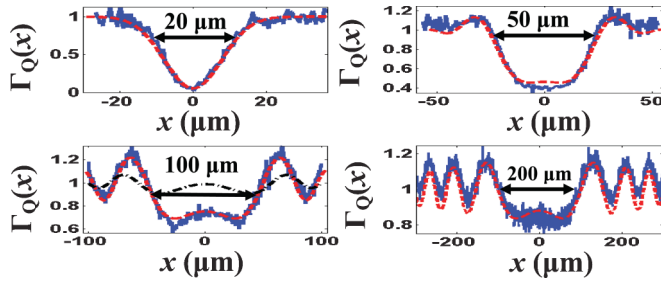


FIG. 2. (Color online) Biphoton dispersion. The four panels show the experimentally measured normalized correlation function [$\Gamma(\tau_0) = R(\tau_0)/R(\infty)$] vs the mirror displacement ($x = \tau_0 c$). (a) No dispersion. The measured dip corresponds to a biphoton temporal width of ~ 40 fs. (b)–(d) Measured dispersion of the biphoton wave packet. For these experiments the dispersive material used is SF11 glass. The glass sample is introduced into paths 3 and 4, while paths 1 and 2 remain empty. The sample lengths in paths 3 and 4 are equal. Panels (b)–(d) correspond to $z_{3,4} = 1, 4, 16$ cm, respectively. In all these figures the blue solid line marks the experimental results while the red dashed line marks the theoretical fitting. In (c) the black dash-dotted line marks the theoretically calculated normalized correlation function for two classical pulses.

Experiments. We use two entangled photons generated from spontaneous parametric down-conversion process in a 5-mm-long type-I BBO crystal, by pumping the crystal with cw light from Ar laser with wavelength 364 nm. The setting was designed to produce two degenerate photons of wavelength 728 nm, and output angles of $\sim 4.15^\circ$. For all the experiments we use SF11 glass as our dispersive medium. First, we measure the interference dip without dispersion. The normalized correlation function $\Gamma(\tau_0) = R(\tau_0)/R(\infty)$ is shown in Fig. 2(a). The width is $\sim 20 \mu\text{m}$, which corresponds to temporal width of $T \approx 40$ fs. Next, we insert two identical glass samples into paths 3 and 4, while leaving paths 1 and 2 empty. In this configuration, both photons effectively pass through the same sample in paths 3 and 4. This means that if one removes the two small Mach-Zehnders (those that split the photons into paths 1 and 2, and 3 and 4), and inserts a dispersive glass into the lower arm of the large Mach-Zehnder interferometer, the same outcome will be measured. In such configuration, if the two photons pass through the lower arm they disperse together, while passing through the upper arm is not accompanied by dispersion at all. According to Eq. (4), we expect the broadening of the dip, fast oscillations, and for strong dispersion—nonzero equal-path visibility. Figures 2(b)–2(d) show the dip for $z_{3,4} = 1, 4, 16$ cm, respectively [blue solid (red dashed) line shows experimental results (theoretical fitting)]. As shown, we indeed observe the broadening of the dip, and the fast oscillations. We find that the GVD coefficient is approximately $\beta^{(2)} \approx 3000 \text{ fs}^2/\text{cm}$. We also find nonzero equal-path visibility. For example, for $z_{3,4} = 4$ cm we find $\mathcal{V}_Q \approx 0.25$. For comparison, we plot in Fig. 2(c) the classical result [Eq. (6)] in black dash-dotted line. Clearly, the equal-path visibility goes to zero, indicating that indeed the Gouy phase for the biphoton wave packet is different than in classical system [in Fig. 2(c) it is always larger than 0.9]. Clearly, the dispersion measurement of the biphoton

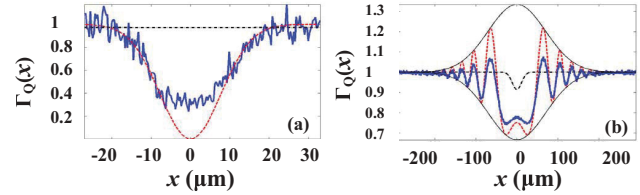


FIG. 3. (Color online) Two cases of dispersion cancellation. Measured normalized correlation function [$\Gamma(\tau_0) = R(\tau_0)/R(\infty)$] vs mirror displacement, x . (a) Dispersion cancellation of the biphoton wave packet. Two glass samples of length $z = 2$ cm are placed in paths 2 and 3, while paths 1 and 4 are left empty. The dip width is as narrow as without the glass samples. The black dashed line marks the theoretical result for the classical pulses, showing dramatic broadening of the classical width. (b) Dispersion reduction of the classical pulses. The black solid outer line marks the envelope of the theoretical fitting. The black dotted line shows the predicted result for classical pulses. Comparison between the width of the dip in the classic system and in the biphoton system shows that the classical dip is much narrower than the dip for the biphoton wave packet. The blue solid line marks the experimental results while the red dashed line marks the theoretical fitting.

wave packet can yield a completely different outcome than the classical measurement in correlation experiments.

Next, we wish to observe the two different regimes: the quantum dispersion cancellation, and the classical reduced dispersion. For the first regime, we choose $z_{2,3} = 2$ cm and $z_{1,4} = 0$ cm. For these lengths, the dispersion of the biphoton is predicted to cancel out, while classically the envelope is expected to broaden. As shown in Fig. 3(a), this is exactly what we measure in the experiments. Blue solid (red dashed) line shows experimental results (theoretical fitting). As can be calculated from Fig. 3(a), the visibility is 0.7, and not 1. This is probably due to misalignment of the system, which results in some distinguishability between the quantum amplitudes. Nevertheless the width of the interference dip is narrow, as without dispersion. For comparison, we also plot the result for the classical pulses in black dash-dotted line in Fig. 3(a). The dip in the classical plot is almost unnoticeable and the visibility approaches zero. For the second regime, where we test classical reduced dispersion, we choose $z_2 = 8$ cm and $z_{1,3,4} = 0$ cm. Now, we expect that the width of the dip will be enhanced, while for the classical pulses the dip's width should be as if dispersion did not occur. Figure 3(b) shows exactly that. The blue solid line shows the experimental results, and the red dashed line is the theoretical fitting. The envelope of the theoretical interference pattern is plotted in black lines. For comparison, we also show the classic result in the black dash-dotted line. The classical width is significantly narrower than the quantum case. Thus, it is possible to change the resulting interference dip from one extreme where the quantum dip is narrower than the classic one, to the other extreme where the classic dip is the narrower one.

Naturally, it is instructive to compare the experiments on the quantum effects presented in Fig. 3 to the corresponding experiments with classical incoherent light. To this end, we use incoherent light with a bandwidth of ~ 33 nm, which corresponds to a coherence time of $T \approx 50$ fs. The light beam is split into the two initial paths of the biphoton, and

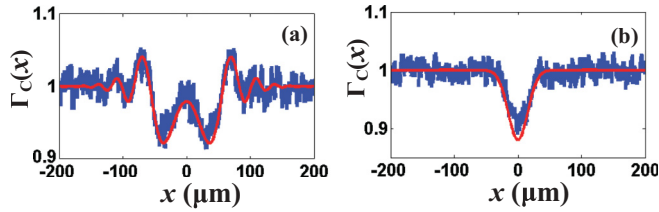


FIG. 4. (Color online) Measured (blue line) and theoretical fitted (red line) normalized correlation function for classical experiments with incoherent light. (a) $z_{1,2} = 0$ and $z_{3,4} = 4$ cm [to compare with Fig. 2(c)]. (b) $z_{1,3,4} = 0$ and $z_2 = 8$ cm [to be compared with Fig. 3(b)].

passes through the exact same experimental system. The results are shown in Fig. 4. For the experimental setup with $z_{1,2} = 0$ and $z_{3,4} = 4$ cm, we find that the classical visibility is $\mathcal{V}_C \approx 0.02$ [shown in Fig. 4(a)] while for biphoton with the same bandwidth it is $\mathcal{V}_Q \approx 0.35$. Comparing this result with the result presented in Fig. 2(c), it is clear that classically the equal path visibility is indeed much lower for the classical light [11]. In Fig. 4(b), we plot the normalized correlation function for $z_{1,3,4} = 0$ and $z_2 = 8$ cm. The width of the classical dip is $x \approx 30 \mu\text{m}$, which is much narrower than the width predicted for the biphoton (hundreds of μm). Comparing Figs. 4(b) and 3(b) shows clearly that, while the biphoton wave packet exhibits significant broadening, the classical light does not exhibit broadening at all.

To summarize, we have shown a coincidence count measurement of GVD of a biphoton wave packet. In our system dispersion can be measured for every propagation length and does not require large propagation distances and/or huge spreading of the packet. We presented a measurement of the Gouy phase of a nonclassical state, and its distinction from the classical case. We pointed to several differences between classical and quantum GVD, among which are the equal-path visibility and the width of the dip. We showed that, under certain parameters, dispersion cancellation can be inverted in such a way that the dip corresponding to classic

field will barely broaden while for a biphoton wave packet it will dramatically increase. The origin of these effects, which differs considerably between classical and biphoton wave packets, is the coherent accumulation of the dispersive phase in the biphotons case which does not happen for classic light (it is the same effect that yields super-resolution with nonclassical light; see Ref. [12]). This collective phase accumulation results in a different evolution of correlated photons in a dispersive medium, compared to the evolution of classic pulses. These results have profound implications in quantum optics, as experiments with entangled photons regularly use interferometry and dispersive materials. The fundamental aspects of dispersion measurement in a quantum system are therefore distinct from those in a classical one, and must be considered carefully in any quantum system containing dispersive elements. Furthermore, if one wants to shape the biphoton wave packet, for various purposes in quantum information and metrology applications, one must be able to control and measure precisely the phase of the biphoton. Since many of the suggested sources of nonclassical light currently can provide only low flux of entangled photons with narrow temporal wave packets, the method suggested here, combined with techniques known to be sensitive to odd order of dispersion [2], can be used for pulse shaping and measurement of such biphoton pulses. Finally, the coherent addition of the dispersion phases can be used to measure properties of narrow samples of materials, since the dispersion acquired by the biphoton is equal to the dispersion accumulated by a classical pulse propagating in the same material for twice the distance. This concept can be extended to entangled states with higher number of photons (NOON states), which will result in accumulating a dispersive phase N times larger than a classical pulse, thereby offering greatly enhanced sensitivity.

This work was supported by the Israel Science Foundation and by the Binational U.S.-Israel Science Foundation. A.B. gratefully acknowledges the financial support of the Israel Clore Foundation.

-
- [1] J. D. Franson, *Phys. Rev. A* **45**, 3126 (1992).
 [2] A. M. Steinberg, P. G. Kwiat, and R. Y. Chiao, *Phys. Rev. Lett.* **68**, 2421 (1992).
 [3] A. Valencia, M. V. Chekhova, A. Trifonov, and Y. Shih, *Phys. Rev. Lett.* **88**, 183601 (2002).
 [4] G. Brida, M. V. Chekhova, M. Genovese, M. Gramegna, and L. A. Krivitsky, *Phys. Rev. Lett.* **96**, 143601 (2006); G. Brida, M. Genovese, L. A. Krivitsky, and M. V. Chekhova, *Phys. Rev. A* **75**, 015801 (2007).
 [5] S. Y. Baek, Y. W. Cho, and Y. H. Kim, *Opt. Express* **17**, 19241 (2009).
 [6] K. A. O'Donnell, *Phys. Rev. Lett.* **106**, 063601 (2011).
 [7] O. Minaeva, C. Bonato, B. E. A. Saleh, D. S. Simon, and A. V. Sergienko, *Phys. Rev. Lett.* **102**, 100504 (2009).
 [8] R. Okamoto, S. Takeuchi, and K. Sasaki, *Phys. Rev. A* **74**, 011801(R) (2006).
 [9] H. Gersen, J. P. Korterik, N. F. van Hulst, and L. Kuipers, *Phys. Rev. E* **68**, 026604 (2003).
 [10] S. Feng and H. G. Winful, *Opt. Lett.* **26**, 485 (2001).
 [11] Note that the biphoton measured in Fig. 3 had a slightly larger bandwidth than the classical light used in Fig. 4. However, the measured differences in the visibility are too large to be explained by the differences in the bandwidth of the classical and quantum light.
 [12] A. N. Boto, P. Kok, D. S. Abrams, S. L. Braunstein, C. P. Williams, and J. P. Dowling, *Phys. Rev. Lett.* **85**, 2733 (2000).